Chemical and electronic characterization of cobalt in Lanthanum perovskites. Effects of Strontium substitution

Jose L. Hueso[1], Juan P. Holgado, Rosa Pereñíguez, Simon Mun[2], Miquel Salmeron[2] and Alfonso Caballero*

Instituto de Ciencia de Materiales de Sevilla (CSIC-University of Seville) and Departamento de Química Inorganica, Universidad de Sevilla. Avda. Américo Vespucio, 49. 41092. Seville, Spain.

[1]Present Address: Department of Chemical Engineering; The University of Texas at Austin, Austin, TX 78712-1062 (USA)

[2]Molecular Foundry. Lawrence Berkeley National Laboratory. Berkeley, CA 94720

** Corresponding author: e-mail: caballero@us.es*

Abstract

Two different cobaltites, $LaCoO_3$ and $La_{0.5}Sr_{0.5}CoO_{3-\delta}$, have been prepared and characterized by means of high energy Co K-edge and low energy O K-edge X-ray absorption spectroscopy (XAS). The partial substitution of La(III) by Sr(II) species induces important changes in the reactivity and electronic state of the perovskite, while little or no changes can be detected in the formal oxidation state of cobalt atoms. The presence of strontium cations induces two main effects in the chemical and electronic behavior of the perovskite. The charge balance with Sr(II) species is reach by the formation of oxygen vacancies throughout the network, which increases the reactivity of the perovskite, now more reducible than the original $LaCoO_3$ perovskite. O K-edge XAS experiments indicate that the Sr(II) species cause *d* electrons of cobalt cations to

change from low to high spin configuration. Our data allow us to propose that this change in spin multiplicity is induced by the bigger size of Sr(II) cations, which aligns the Co-O-Co atoms, and favors the overlapping of π-symmetry cobalt and oxygen orbitals, reducing the splitting energy of e_g and t_{2g} levels.

Keywords:

Cobaltites, perovskites, In-situ XAS, EXAFS, XANES, NEXAFS, Crystal field splitting

1. Introduction

Oxides with perovskite structure (ABO_3), where A and B are metallic cations of different sizes, are of scientific interest because of their relevant electric, magnetic or catalytic properties (1-6). Many papers have been published in recent years related to the partial substitution of atoms A and/or B, which allows for a controlled modification of most of these properties. Strontium-substituted lanthanum cobalt and others oxides with perovskites structure ($La_{1-x}Sr_xCoO_{3-\delta}$) have been extensively investigated in last years because of their relevant magnetic properties (some of them exhibiting giant magnetoresistance at low temperatures (7)), or its use as cathode material in high temperature fuel cells (8,9). They are also interesting for their catalytic properties in the oxidation of hydrocarbon and soots, and the decomposition of nitrogen oxides (10). Moreover, some authors have found that the low spin configuration of the $LaCoO_3$ perovskite at room temperature changes to a higher spin configuration by increasing the temperature or introducing Sr(II) atoms, also associated with changes in magnetic and conducting properties (11-15). In spite of that, there is no general agreement about the origin of these relevant characteristics. So, while some authors suggest that these new properties are induced by Co(IV) ions stabilized in the Strontium-substituted

perovskites, others attribute them exclusively to the generation of oxygen vacancies compensating the divalent charge of Sr atoms (9,16,17).

The aim of our research has been to clarify the chemical and electronic modifications induced by this Strontium-substitution by means of X-ray absorption spectroscopies. The combined study of the high energy Co K-edge (Extended X-ray absorption spectroscopy, EXAFS, and X-ray absorption near-edge structure, XANES) and the low energy O-K edge X-ray absorption spectroscopy (XAS) have shed some light on the oxidation states, the spin configurations and the chemical reactivity of $LaCoO_3$ and $La_{0.5}Sr_{0.5}CoO_{3-\delta}$ perovskites.

2. Experimental

2.1. Preparation method

The perovskite catalysts used for the present investigation, $La_{0.5}Sr_{0.5}CoO_{3-\delta}$ and $LaCoO_3$, were synthesized by spray pyrolysis (18,19). The preparation method involved the uniform nebulisation of nitrate solutions containing $La(NO_3)_3 \cdot 6H_2O$ (99.99%, Aldrich), $Co(NO_3)_2 \cdot 6H_2O$ (>98%, Fluka), and $Sr(NO_3)_2$ (>99%, Fluka) prepared as a 0.1 M liquid solution of precursors. Two online furnaces, at 250 and 600ºC, evaporated the solvent (distilled water) with the dissolved nitrates and produced an initially amorphous perovskite powder. The material was collected by a porous quartz frit located at the outlet of the heating system. Then the amorphous powders were annealed at 700ºC for 4 h, thus obtaining $LaCoO_3$ and $La_{0.5}Sr_{0.5}CoO_{3-\delta}$ crystalline perovskites with rhombohedral symmetry (19).

2.2. Characterization techniques

XRD analysis of the samples before and after treatment was performed in a Siemens D-500 diffractometer working in a Bragg-Bentano configuration and using a Cu anode under an applied voltage of 36 kV and current of 26 mA. XRD spectra were recorded with a step size of 0.02 degrees and an accumulation time of 10 s per step.

Temperature Programmed Reduction (TPR) experiments were done on a H_2/Ar mixture (5% H_2, 50 ml/min flow) from room temperature up to 750ºC, with a heating rate of 10 K/min. The experimental conditions were chosen to assure that no peaks coalescence occurs (20). A thermal conductivity detector (TCD), previously calibrated using CuO, and a mass spectrometer in line with the TCD, calibrated with reference mixtures, were used to detect variations of H_2 concentration, and possible sub-products formation.

High energy X-ray absorption spectra (XAS) were recorded at the BM25 beam line (SPLINE) of the ESRF synchrotron (Grenoble, France). The spectra were acquired in transmission mode with a modified commercial infrared cell (Specac), using self-supported wafers of the perovskite samples. XAS spectra (EXAFS and XANES regions) were collected at room temperature after the treatments indicated in each case. In all cases the pellets were prepared using the optimum weight to maximize the signal-to-noise ratio in the ionization chambers (log $I0/I1 \approx 1$). Mass flow controllers were used for dosing the gases to the cell, using a total flow of 100 ml/min. The composition of the gas mixtures were similar to that previously used in the TPR experiment, for the hydrogen reduction and reoxidation treatments. For energy calibration, a standard Co foil was introduced after the second ionization chamber ($I1$) and measured simultaneously. Typical XAS spectra of Co K-edge were recorded from 7500 to 8700 eV, with a variable step energy value, with a minimum 0.5 eV step across the XANES region. Once extracted from the XAS spectra, the EXAFS oscillations were Fourier

transformed in the range 2.0–12.0A^{-1}. In some cases, spectra were analyzed/simulated using the software package IFEFFIT (21). The theoretical paths for Co–Co and Co–O species used for fitting the first coordination shell of the experimental data were generated using the FEFF 7.0 program (22). The coordination numbers, interatomic distance, Debye–Waller factor and inner potential correction were used as variable parameters for the fitting procedures. Reference spectra for CoO, Co_3O_4 and metallic Co were recorded using standard reference samples.

Low energy X-ray Absorption spectra (XAS) at the O *K*-edge were collected at the beamline 9.3.2 of the Advanced Light Source (ALS) at Lawrence Berkeley National Laboratory. The energy resolution was about 3000 at the oxygen *K* edge. The base pressure of the chamber during the experiments was better than 10^{-8} torr.

3. Results and Discussion

3.1. Structural and chemical characterization of cobaltites

After the spray pyrolysis preparation, the two samples, $LaCoO_3$ and $La_{0.5}Sr_{0.5}CoO_{3-\delta}$, were amorphous. However, after calcination at 600ºC the XRD patterns were in both cases characteristics of well crystallized rombohedrical structures (R-3C) with no presence of other minority phases (19).

The XANES spectra of these two samples before and after calcination are displayed in Figure 1. The spectra of Co_3O_4 and CoO are also shown as references. Before calcination, both samples show an oscillation pattern after the main peak (E>7730eV) similar to that of cobalt spinel reference, indicating that these amorphous samples have the same short-range structure as this cobalt oxide. This conclusion agrees with the magnitude of the F.T. peaks obtained from the EXAFS spectra (Figure 2a) where the two cobaltites and the cobalt spinel present the 3 main peaks (around 1.5, 2.5

and 3.0 A) centered at the same distances. The third peak is much less intense for the two cobaltites, in agreement with the amorphous state detected by XRD. A FEFF simulation of the cobalt spinel structure (23) is included in Figure 3. This calculation shows that the three main peaks appearing in the radial distribution function of the amorphous cobaltites can be reproduced with just 4 coordination shells around the tetrahedral and octahedral cobalt atoms in the spinel structure. That means that spinel-type ordered domains of around 7A are present in these amorphous cobaltites. Remarkably, the edge of the two samples (Figure 1a) are shifted to a higher energy than the cobalt spinel, indicating that the mean oxidation state of cobalt is higher in the cobaltites, and closer to Co(III) species.

After calcination, the XANES spectra of the cobaltites evolve to that presented in Figure 1b, which are similar to those obtained previously by others authors for perovskite structures (7,16). The oscillations after the edge are now clearly different from the two cobalt oxide references, and the energy of the edges, both at the same position, are further shifted to higher energy. This energy must corresponds to Co(III) species and so, contrary to the proposal of others authors (24), no evidence for the stabilization of Co(IV) states can be found in this XANES spectrum for the strontium substituted cobaltite $La_{0.5}Sr_{0.5}CoO_{3-\delta}$. As a result, the differences in the cationic charges of La(III) and Sr(II) should be mainly compensated by oxygen vacancies in the perovskite framework, which would imply a maximum value of 0.25 for the δ stoichiometric factor of the Strontium-substituted perovskite. These changes in XANES spectra come with major modifications in the F.T. magnitude of the EXAFS spectra (Figure 4b), resulting in radial distribution functions similar to those reported previously for perovskite structures (9). The overlapping peaks in the 3-4A range are much less intense for the Sr-substitute cobaltite, which must be due to a sort of structural disorder

caused by the oxygen vacancies present in this compound. Also, it cannot be discarded that the simultaneous presence of Sr and La in the second coordination shell of cobalt induces interferences leading to the less intense peak observed in the F.T. magnitude function.

3.2. Reactivity changes induced by Sr

As mentioned before, the insertion of Sr(II) atoms in the "A" position of ABO_3 perovskites was primarily intended to increase the reactivity of the original $LaCoO_3$ cobaltite by inducing changes in the cobalt oxidation state and/or the formation of oxygen vacancies, as a result of the presence of Sr(II) species substituting the La(III) atoms. Differences in reactivity have become evident in the TPR profiles included in Figure 4. After calcination at 500ºC (first TPR) the Sr- containing sample is completely reduced, while the $LaCoO_3$ need to be heated to at least 600ºC in hydrogen. After reoxidation at 500ºC, the new reduction experiments (second TPR) show modified profiles, which do not correspond to those obtained for the references of cobalt oxides. In all cases, the consumption of hydrogen corresponds to the total reduction from Co(III) to Co(0) species. To further elucidate the structural changes involved in these reduction and reoxidation treatments, an *in situ* XAS study has been accomplished over these two cobaltites.

Figure 5 shows the XANES spectra for the $LaCoO_3$ sample submitted to a reduction treatment in hydrogen at 500ºC, followed by a reoxidation at the same temperature. It can be observed as upon reduction, the edge of the XANES spectrum is shifted to lower energy, but higher than that of CoO, indicating that the cobalt has been only partially reduced to Co(II) species. However, no important changes can be observed in the oscillation pattern after the edge, showing that no major structural

changes have occurred in the perovskite structure. Finally, after reoxidation at 500ºC an almost identical spectrum is obtained, with the same edge energy as the original sample. The magnitude of the F.T. peaks from the EXAFS spectra (Figure 6) brings about the same conclusions. Only changes in the intensity of the main peaks are detected after reduction at 500ºC, while maintaining the same original R values. The subsequent reoxidation at 500ºC restores the intensity of the first peak (Co-O first coordination shell), while the peaks around 3-4A is only slightly recovered, reaching an intensity similar to the Sr-substituted perovskites. So, XAS spectroscopy shows as cobalt is partially reduced to Co(II) but the perovskite framework remains unchanged. After reoxidation the Co(III) state is recovered but a completely ordered perovskite network is not fully restored.

As expected from the TPR profile of Figure 4, the XANES spectra (Figure 7) indicates that the Sr-substituted cobaltite is almost completely reduced to the metallic state upon treatment in hydrogen at 500ºC. Also, the main peak at 2.2A in the F.T. (Figure 8) comes from Co-Co distances of metallic cobalt, and only the weak shoulder at 1.6A reveals some remains of oxidized cobalt. Remarkably, the subsequent reoxidation treatment produces a cobalt oxide phase with notable differences and resemblances with the reference of cobalt spinel. While the F.T. shows a radial distribution function similar to the cobalt spinel, the XANES indicates that cobalt is much more oxidized, according to the higher energy of the edge. Again, the oscillations after the edge are similar to that of the spinel. These findings show that a highly oxidized spinel structure is stabilized after this reduction and reoxidation treatments. It is important to stress that at this stage, although less intense than the original sample, the main component detected by XRD is again a perovskite phase (Figure 9) and only

very weak peaks from a spinel phase are present in the diagram, indicating that the spinel-like phase detected by Co K-edge XAS must remains amorphous.

3.3. Crystal field effects upon Sr-substitution

Scheme 1 shows a simplified Molecular Orbital diagram corresponding to cobalt coordinated by oxygen in an octahedral environment, as that present in the perovskite structure. As can be seen, the overlap between O 2p levels and Co 3d orbitals splits them in t_{2g} and e_g levels. It is known that, depending on the overlap the electronic structure of d^6 Co(III) species could correspond to a low spin ($t_{2g}^6 e_g^0$) or to a higher spin states ($t_{2g}^5 e_g^1$ or $t_{2g}^4 e_g^2$), although Co(III) compounds in a octahedral environment of oxygen have normally low spin configurations. From this scheme it is obvious that, as has been proposed previously (9), the O K-edge XAS spectra can be used to evaluate the nature of the crystal field splitting in this kind of compounds.

Figure 10 shows the O K-edge XAS spectra of our two cobaltites, $LaCoO_3$ and $La_{0.5}Sr_{0.5}CoO_{3-\delta}$. According to the literature (9,11,25) the features in the energy range of 525eV-539eV are mainly produced by transitions of the O 1s electrons to the Co 3d levels of cobalt, which are extensively mixed with the O 2p states. As depicted in the figure, at higher energy the La 5d, Co 4s and 4p levels are also involved in the O K-edge spectra. As shown in Figure 10 (right), the 525-539eV region of the $LaCoO_3$ XAS is dominated by a main peak centered at around 529.6eV, while in the Sr-substituted XAS arises a new peak at 527.6eV. As stated before by other authors (7,11,12), this new feature, separated 2.1eV from the fist one, is a consequence of a transition from a low spin state, presents in the $LaCoO_3$, to a high spin configuration, when Sr atoms are introduced in the network, allowing the electron transition to the now partially empty t_{2g} levels. This change in the spin multiplicity has been explained previously considering

that the presence of Sr(II) species induces the oxidation of cobalt to Co(IV), resulting in a $t_{2g}^5e_g^1$ or a $t_{2g}^4e_g^2$ electronic configuration, even though it is well known that, according to the ligand field theory (26), higher oxidation states favors low spin configurations in the splitted d orbitals.

As stated before, our XAS study allow us to suggest that the formal oxidation state of cobalt is mainly Co(III) in the two perovskites. So, changes in total positive charge produced by introducing Sr(II) species must be compensated just or mainly by oxygen vacancies in the perovskite framework.

From a chemical point of view, the observed change in the spin state of the cobalt in the perovskite induced by strontium could be explained just with structural considerations. As depicted in scheme 2, the higher ionic radius of Sr(II), 1.58A vs. 1.50A for La(III) (27) can reduces the rombohedrical distortion of the perovskite structure. In fact, the structural data included also in the scheme, obtained from XRD data (10) show a higher Co-Co distance in the Sr-substituted perovskite, compatible with a small expansion of the cell. This distance is closer to twice the Co-O distance in the $[CoO_6]$ octahedron, showing that, as recognized recently by other authors (13), the Co-O-Co bond angle has increased, approaching the ideal 180^o in cubic structures. As a result, almost no distortion occurs in the rombohedrical structure of the $La_{0.5}Sr_{0.5}CoO_{3-\delta}$ substituted perovskite. Considering that the Co-O distances remain unchanged by Sr-substitution, no modification of Co-O σ-interaction must be expected. However, a better alignment of Co-O-Co atoms in two adjacent octahedrons will favor mainly the overlapping of the cobalt and oxygen orbitals with π symmetry. It is well known in chemistry that, according to the ligand field theory, this is an important factor determining the crystal field splitting of *d* levels with a π-donor ligand like $O^=$ species in oxides (26). As a consequence, the presence of Sr(II) will induce a decrease in the

crystal field (scheme 3) favoring the high spin electronic configuration observed in the NEXAFS spectra.

4. Conclusions

In summary, we have presented an XAS study of $LaCoO_3$ and $La_{0.5}Sr_{0.5}CoO_{3-\delta}$ perovskites at the Co K-edge and O K-edge. This study has shown that partial substitution of La(III) cations by Sr(II) divalent species produces important changes in chemical reactivity and electronic configuration, while no changes can be measured in the oxidation state of cobalt atoms. The creation of oxygen vacancies in the perovskite structure increases the reactivity of the perovskite, making it easier to reduce the solid to metallic cobalt. By reoxidation of the previously reduced $La_{0.5}Sr_{0.5}CoO_{3-\delta}$, a highly oxidized spinel-like phase has been obtained.

The results from O K-edge XAS indicate that the spin configuration of cobalt in the Sr-substituted changes from an initial high field, low spin state to a low field high spin configuration. The results obtained from the Co K-edge XAS indicate that little or no changes are produced in the formal oxidation state of cobalt, which remains as a trivalent specie in the Sr-containing perovskite. All these results lead us to propose that changes in spin configuration of Co(III) can be explained just considering the better alignment of Co-O-Co atoms caused by the larger size of Sr(III). The resulting increase in volume favors a better overlapping between cobalt and oxygen π-type orbitals, which produces an increase in the energy of t_{2g} levels and the concomitant decrease in the ligand field splitting of Co *d* orbitals.

Acknowledgements

We thank the Ministry of Science and Education of Spain for financial support (Projects ENE2004-01660 and ENE2007-67926-C02-01). We also thank the staff of the ESRF BM25 beamline and ESRF facility (Grenoble, France) and the staff of ALS beamline 9.3.2 and ALS facility (LNBL, Berkeley, CA) for funding and helping to accomplish these experiments. MS is funded by the Office of Basic Energy Sciences, Chemical Sciences, Geosciences, and Biosciences Division, under the Department of Energy Contract No. DE-AC02-05CH11231.

References

(1) Peña, M. A.; Fierro, J. L. G. *Chem. Rev.* **2001,** *101,* 1981-2017.

(2) Nishihata, Y.; Mizuki, J.; Akao, T.; Tanaka, H.; Uenishi, M.; Kimura, M.; Okamoto, T.; Hamada, N. *Nature* **2002,** *418,* 164-167.

(3) Tanaka, H.; Misono, M. *Curr. Op. Sol.St.Mat.Sci.* **2001,** *5,* 381-387.

(4) Kimura, S.; Maeda, Y.; Kashiwagi, T.; Yamaguchi, H.; Hagiwara, M.; Yoshida, S.; Terasaki, I.; Kindo; K. *Phys. Rev. B* **2008,** *78,* 180403(R).

(5) Rijssenbeek, J. T.; Saito, T.; Malo, S.; Azuma, M.; Takano, M.; Poeppelmeier, K. R. *J. Am. Chem. Soc.* **2005,** *127,* 675-681.

(6) Margadonna, S.; Karotsis, G. *J. Am. Chem. Soc.* **2006,** *128,* 16436-16437.

(7) Toulemonde, O.; N`Guyen, N.; Studer, F. *J. Sol. St. Chem.* **2001,** *158,* 208-217.

(8) Bellino, M. G.; Sacanell, J. G.; Lamas, D. G.; Leyva, A. G.; Walse de Reca, N. E. *J. Am. Chem. Soc.* **2007,** *129,* 3066-3067.

(9) Haas, O.; Struis, R. P. W. J.; McBreen, J. M. *J. Sol. St. Chem.* **2004,** *177,* 1000-1010.

(10) Hueso, J. L.; Caballero, A.; Ocaña, M.; Gonzalez-Elipe, A. R. *J. Catal.* **2008,** *257,* 334-344.

(11) Abbate, M.; Fuggle, J. C.; Fujimori, A.; Tjeng, L. H.; Chen, C. T.; Potze, R.; Sawatzky, G. A.; Eisaki, H,; Uchida, S. *Phys. Rev. B* **1993,** *47,* 16124-16130.

(12) Moodenbaugh, A. R.; Nielsen, B.; Sambasivan, S.; Fisher, D. A.; Friessnegg, T.; Aggarwal, S.; Ramesh, R.; Pfeffer, R. L. *Phys. Rev. B* **2000,** *61,* 5666.

(13) Efimova, E.; Efimov, V.; Karpinsky, D.; Kuzmin, A.; Purans, J.; Sikolenko, V.; Tiutiunnikov, S.; Troyanchuk, I.; Welter, E.; Zajac, D.; Simkin, V.; Sazonov, A. *J. Phys. Chem. Solids* **2008,** *69,* 2187-2190.

(14) Pinta, C.; Fuchs, D.; Merz, M.; Wissinger, M.; Arac, E.; Löhneysen, H. v.; Samartsev, A. *Phys. Rev. B* **2008,** *78,* 174402.

(15) Haverkort, M. W.; Hu, Z.; Cezar, J. C.; Burnus, T.; Hartmann, H.; Reuther, M.; Zobel, C.; Lorenz, T.; Tanaka, A.; Brookes, N. B.; Hsieh, H. H.; Lin, H. –J.; Chen, C. T.; Tjeng L. H. *Phys. Rev. Letters* **2006,** *97,* 176405.

(16) Hanashima, T.; Azuhata, S.; Yamawaki, K.; Shimizu, N.; Mori, T. Tanaka, M.; Sasaki, S. *Jap. J. Appl. Phys.* **2004,** *43,* 4171-4178.

(17) Sunstrom IV, J. E.; Ramanujachary, K. V.; Greenblatt, M.; Croft, M. *J. Sol. Stat.Chem.* **1998,** *139,* 388-397.

(18) Hueso, J. L.; Cotrino, J.; Caballero, A.; Espinos, J. P.; Gonzalez-Elipe, A. R. *J. Catal.* **2007,** *247,* 288-297.

(19) Lopez-Navarrete, E.; Caballero, A.; Orera, V. M.; Lazaro, F. J.; Ocaña, M. *Acta Mater.* **2003,** *51,* 2371-2381.

(20) Malet, P.; Caballero, A. *J. Chem. Soc. Faraday Trans.* **1988,** *84,* 2369-2375.

(21) Newville, M. *J. Synchr. Rad.* **2001,** *8,* 322-324.

(22) Ankudinov, A. L.; Rehr, J. J. *Phys. Rev. B* **1997,** *56,* 1712.

(23) Holgado, J. P.; Caballero, A.; Espinos, J. P.; Morales, J.; Jimenez, V. M.; Justo, A. *Thin Solid Films* **2000,** *377,* 460-466.

(24) Berry, F. J.; Marco, J.F.; Ren, X. *J. Sol. State Chem.* **2005,** *178,* 961-969.

(25) Abbate, M.; de Groot, F. M. F.; Fuggle, J. C.; Fujimori, A.; Strebel, O.; Lopez, F.; Domke, M.; Kaindl, G.; Sawatzky, G. A.; Takano, M.; Takeda, Y.; Eisaki, H.; Uchida, S. *Phys. Rev. B* **1992,** *46,* 4511.

(26) Ballhausen, C. J. *"Introduction to Ligand Field Theory"* **1962,** McGraw-Hill, New York; Figgis, B. N.; Hitchman, M. A. *"Ligand Field Theory and Its Applications"* **2000,** Wiley-VCH.

(27) Shannon, R. D. *Acta Crystallograhica A* **1976,** *32,* 751-767.

Figure captions

Figure 1. Co K-edge XANES spectra of Lanthanum Cobaltites (a) before and (b) after calcination at 600°C.

Figure 2. F.T. of the Co K-edge EXAFS spectra of Lanthanum Cobaltites (a) before and (b) after calcination at 600°C.

Figure 3. FEFF simulation of the atomic environment around octahedral (O_h) and tetrahedral (T_d) cobalt atoms of Co_3O_4. The numbers at each curve refer to the number of coordination shells in the clusters for tetrahedral Co(II) and octahedral Co(III) ions.

Figure 4. Temperature-programmed reduction (TPR) profiles of Lanthanum Cobaltites calcined at 600°C (left) and reoxidized after the first TPR (right).

Figure 5. *In situ* Co K-edge XANES spectra of $LaCoO_3$. All the spectra have been collected *in situ* at room temperature after the indicated treatments.

Figure 6. F.T. of the *In situ* Co K-edge EXAFS spectra of $LaCoO_3$. All the spectra have been collected *in situ* at room temperature after the indicated treatments.

Figure 7. *In situ* Co K-edge XANES spectra of $La_{0.5}Sr_{0.5}CoO_{3-\delta}$. All the spectra have been collected *in situ* at room temperature after the indicated treatments.

Figure 8. F.T. of the *In situ* Co K-edge EXAFS spectra of $La_{0.5}Sr_{0.5}CoO_{3-\delta}$. All the spectra have been collected *in situ* at room temperature after the indicated treatments.

Figure 9. XRD diagrams of $La_{0.5}Sr_{0.5}CoO_{3-\delta}$ calcined at 600°C (left) and reoxidized after reduction at 500°C (right).

Figure 10. (a) O K-edge X-ray absorption spectra of Lanthanum Cobaltites. (b) Co 3d bands region of the O K-edge X-ray absorption spectra.

Scheme 1. Simplified molecular orbital diagram of Co(III) ions in a octahedral environment.

Scheme 2. Substitution of La(III) ions by the larger Sr(II) ions induces changes in the cubic environment of A atoms of ABO_3 perovskites. The geometry changes modify the orientation and overlapping of Co and O π-symmetry type orbitals.

Scheme 3. Simplified molecular orbital diagram of Co(III) ions in a octahedral environment. Interaction with electronegative π-donor ligands reduces the d orbital splitting (right). The higher the π-interaction, the lower the orbital splitting (right), which favors high spin electronic configurations.

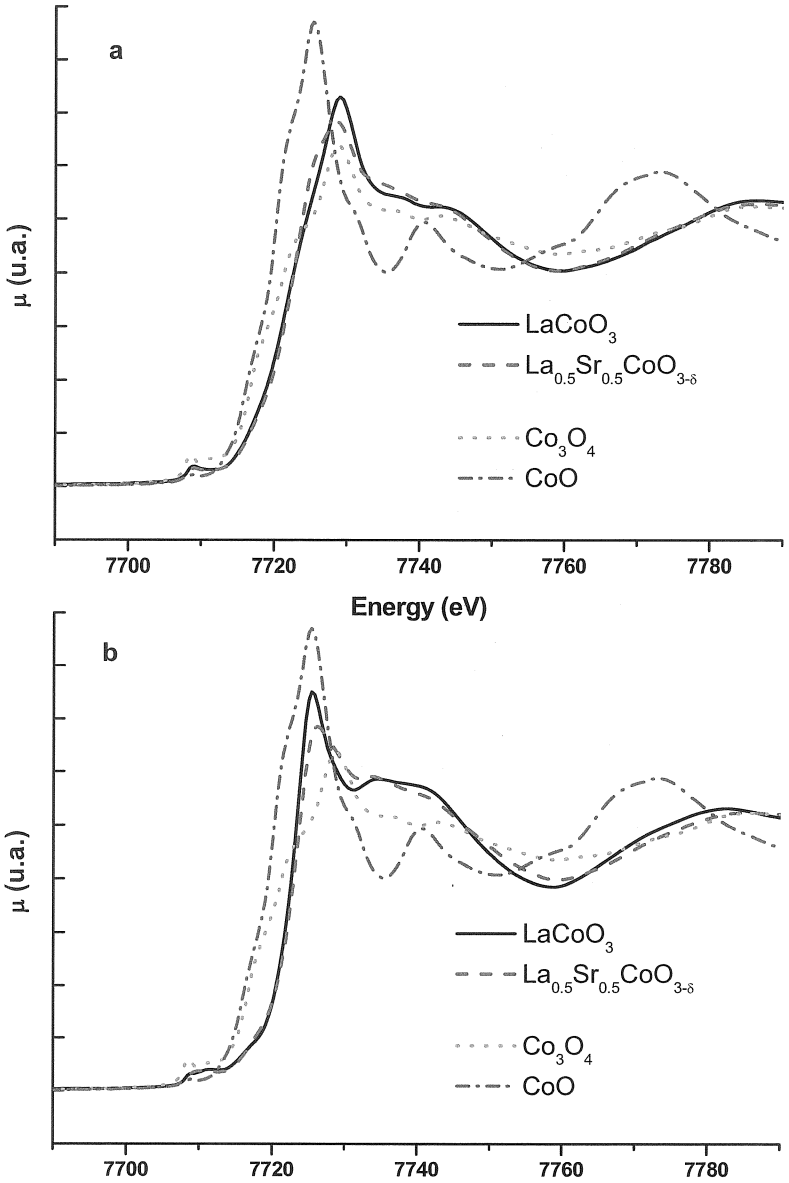
a
μ (u.a.)
LaCoO3
La0.5Sr0.5CoO3-δ
Co3O4
CoO
7700
7720
7740
7760
7780
Energy (eV)
b
μ (u.a.)
LaCoO3
La0.5Sr0.5CoO3-δ
Co3O4
CoO
7700
7720
7740
7760
7780

Figure 1

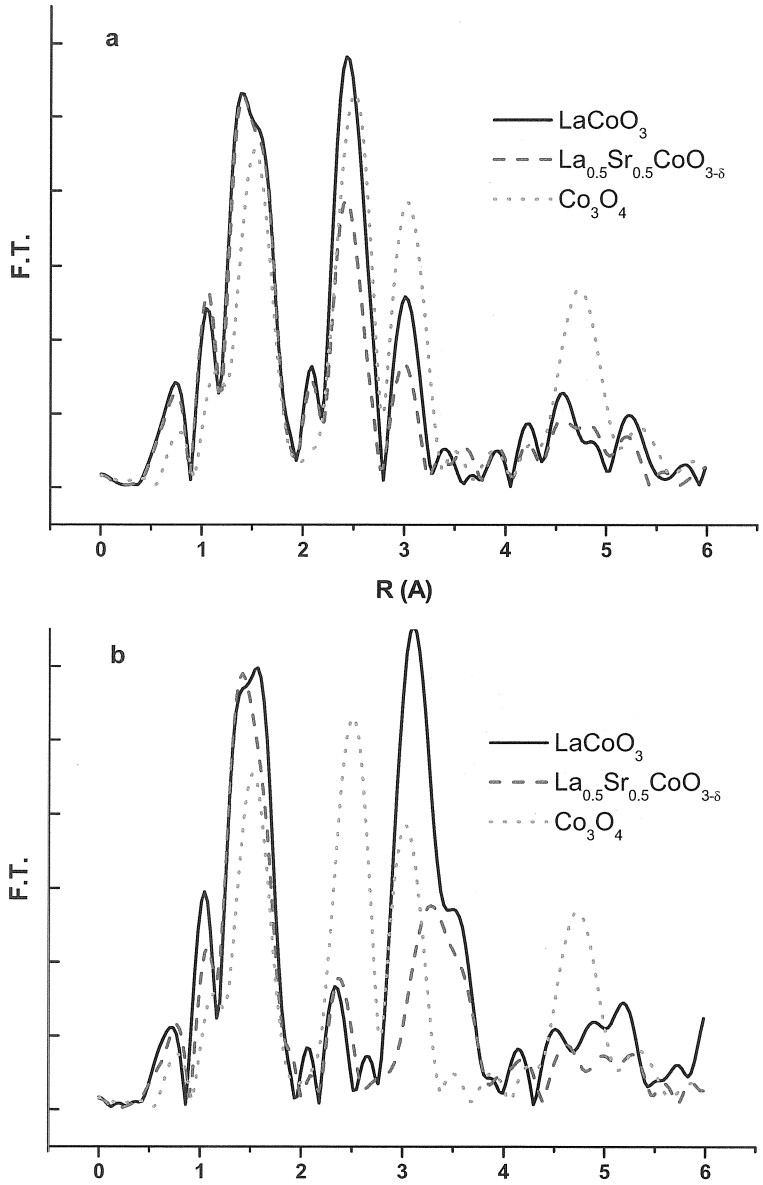
a
F.T.
LaCoO3
La0.5Sr0.5CoO3-δ
Co3O4
0
1
2
3
4
5
6
R (A)
b
F.T.
LaCoO3
La0.5Sr0.5CoO3-δ
Co3O4
0
1
2
3
4
5
6

Figure 2

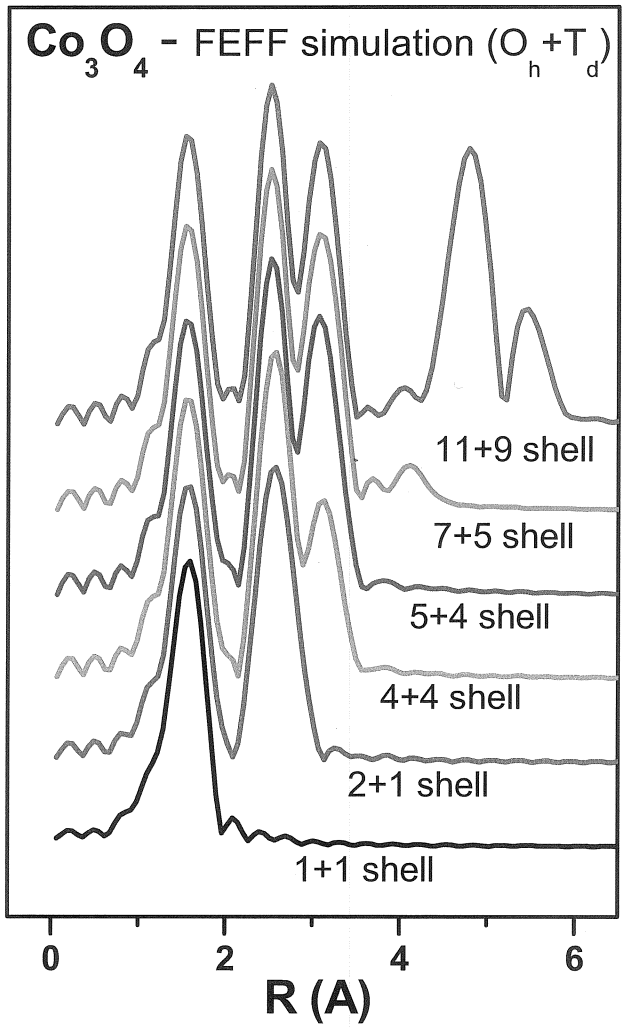
Co3O4 - FEFF simulation (Oh+Td)
11+9 shell
7+5 shell
5+4 shell
4+4 shell
2+1 shell
1+1 shell
0
2
4
6
R (A)

Figure 3

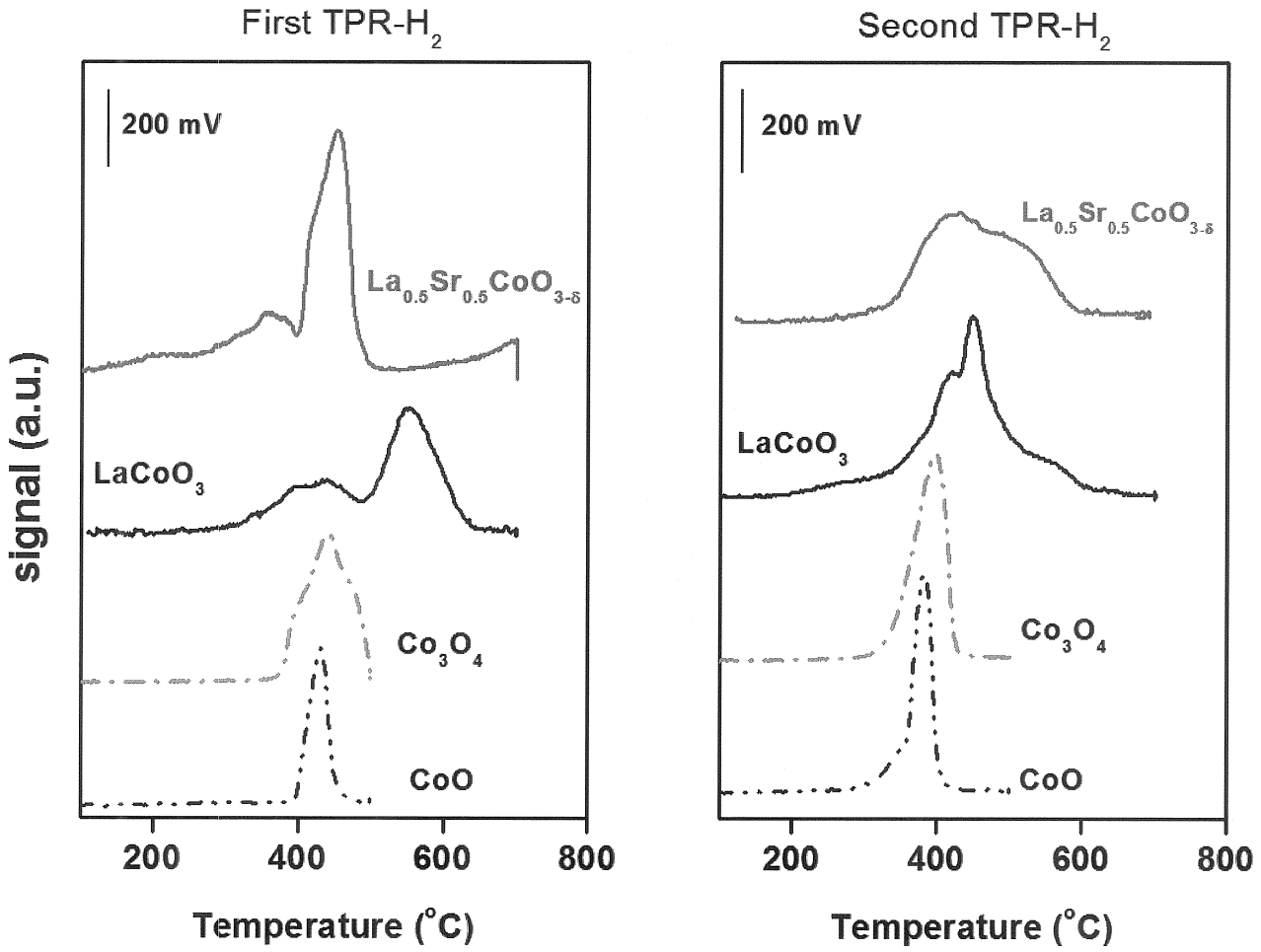
First TPR-H2
Second TPR-H2
200 mV
200 mV
La0.5Sr0.5CoO3-δ
La0.5Sr0.5CoO3-δ
LaCoO3
LaCoO3
Co3O4
Co3O4
CoO
CoO
signal (a.u.)
200
400
600
800
200
400
600
800
Temperature (°C)
Temperature (°C)

Figure 4

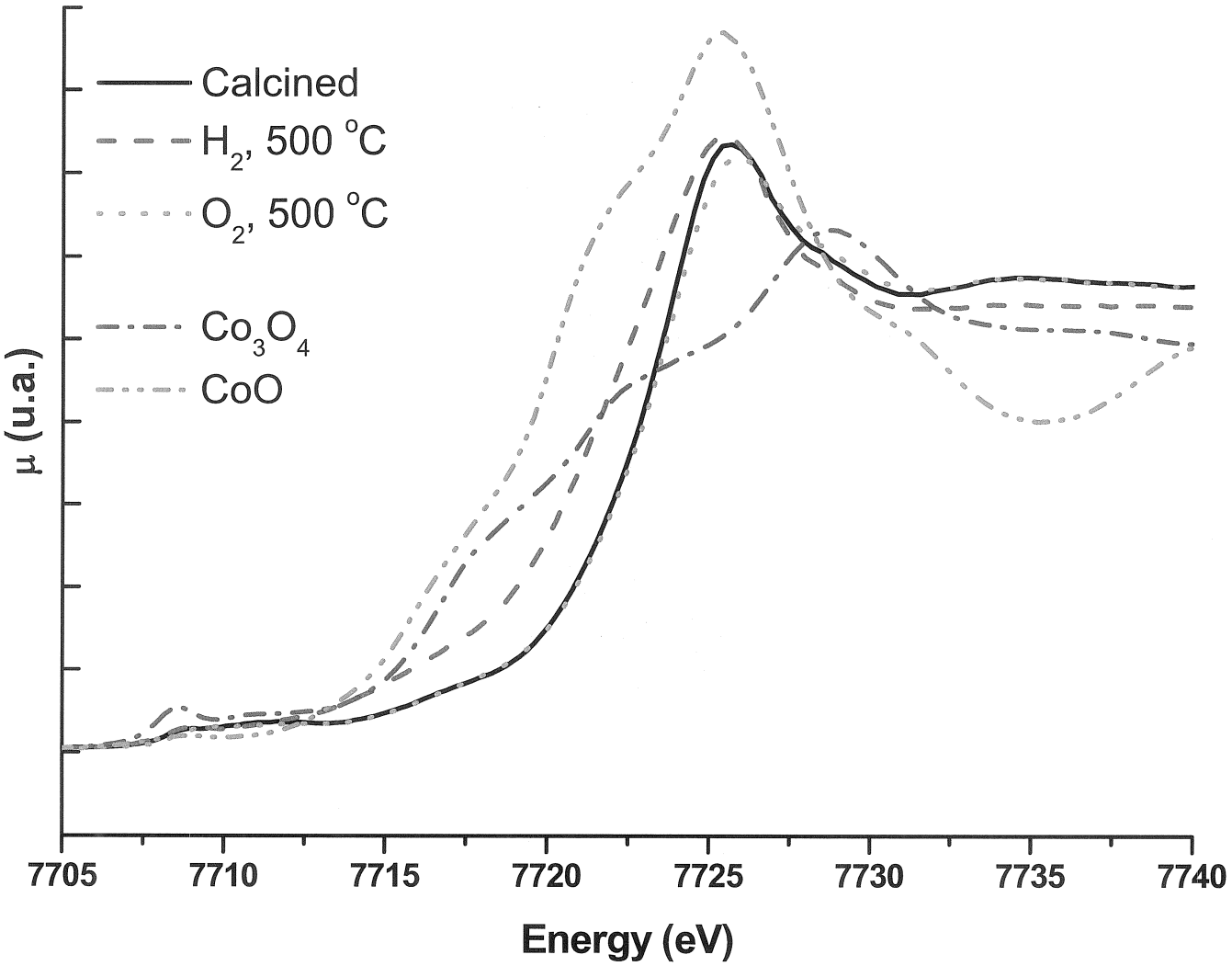
Calcined
H2, 500 °C
O2, 500 °C
Co3O4
CoO
μ (u.a.)
7705
7710
7715
7720
7725
7730
7735
7740
Energy (eV)

Figure 5

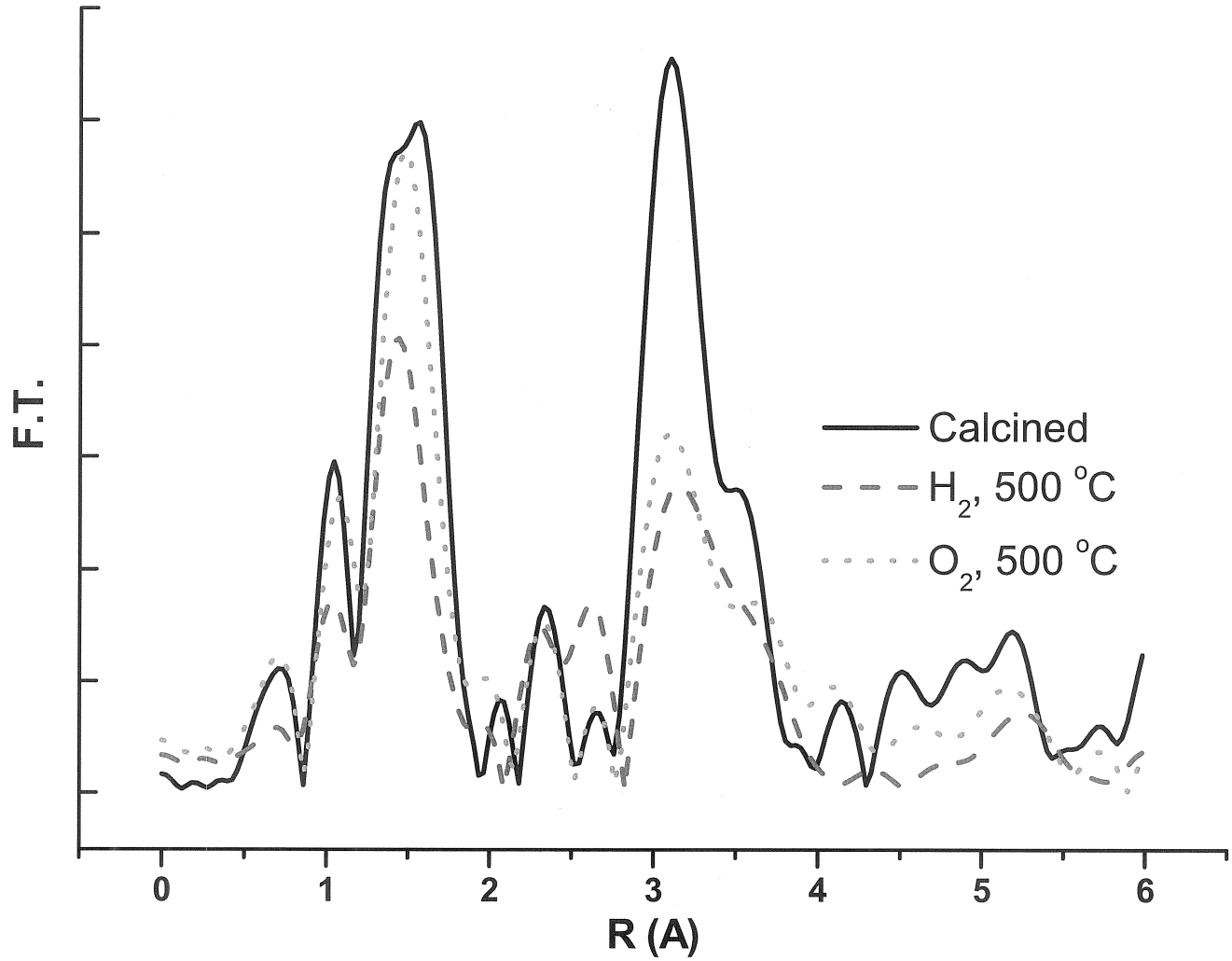

Figure 6

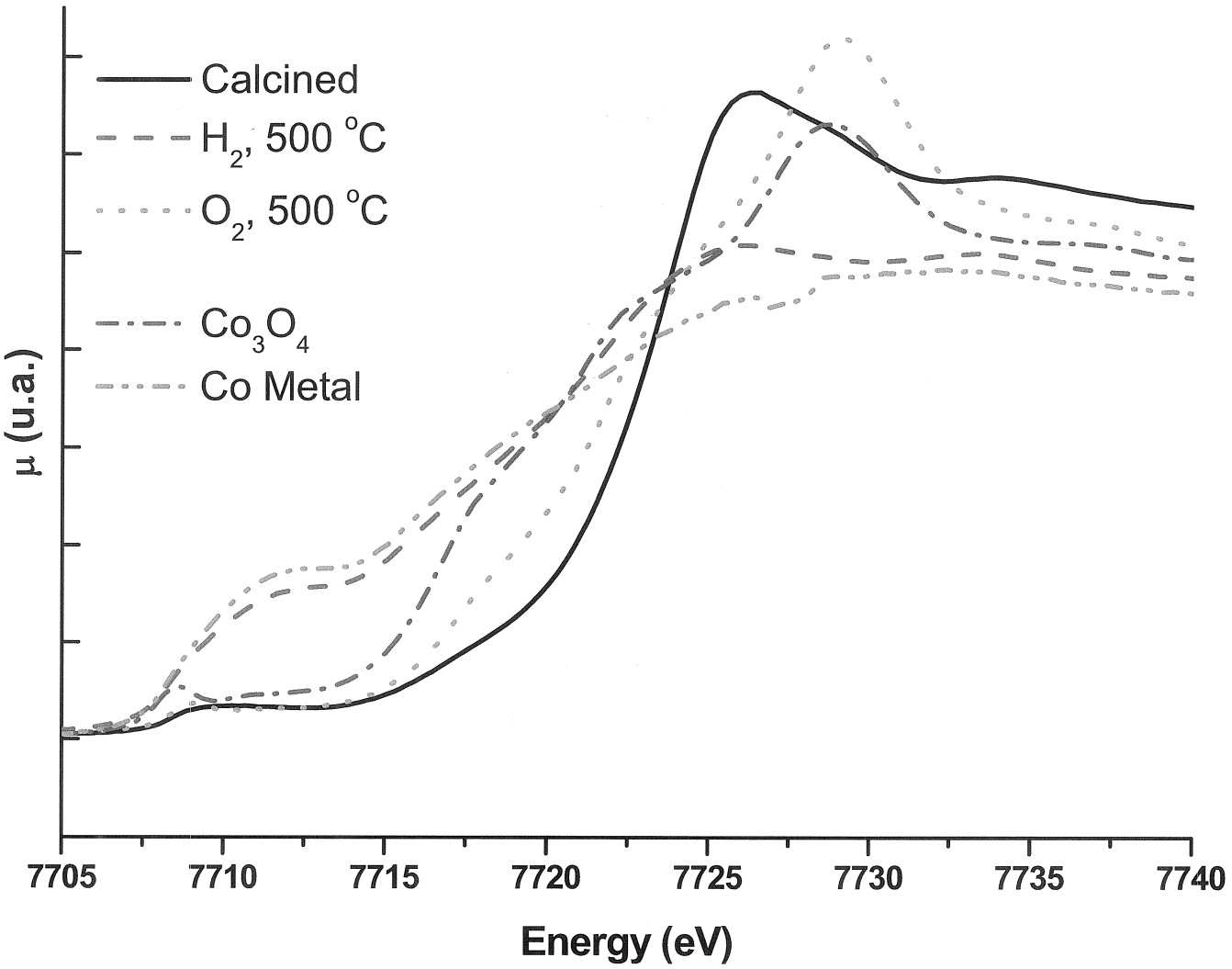
Calcined
H2, 500 °C
O2, 500 °C
Co3O4
Co Metal
μ (u.a.)
7705
7710
7715
7720
7725
7730
7735
7740
Energy (eV)

Figure 7

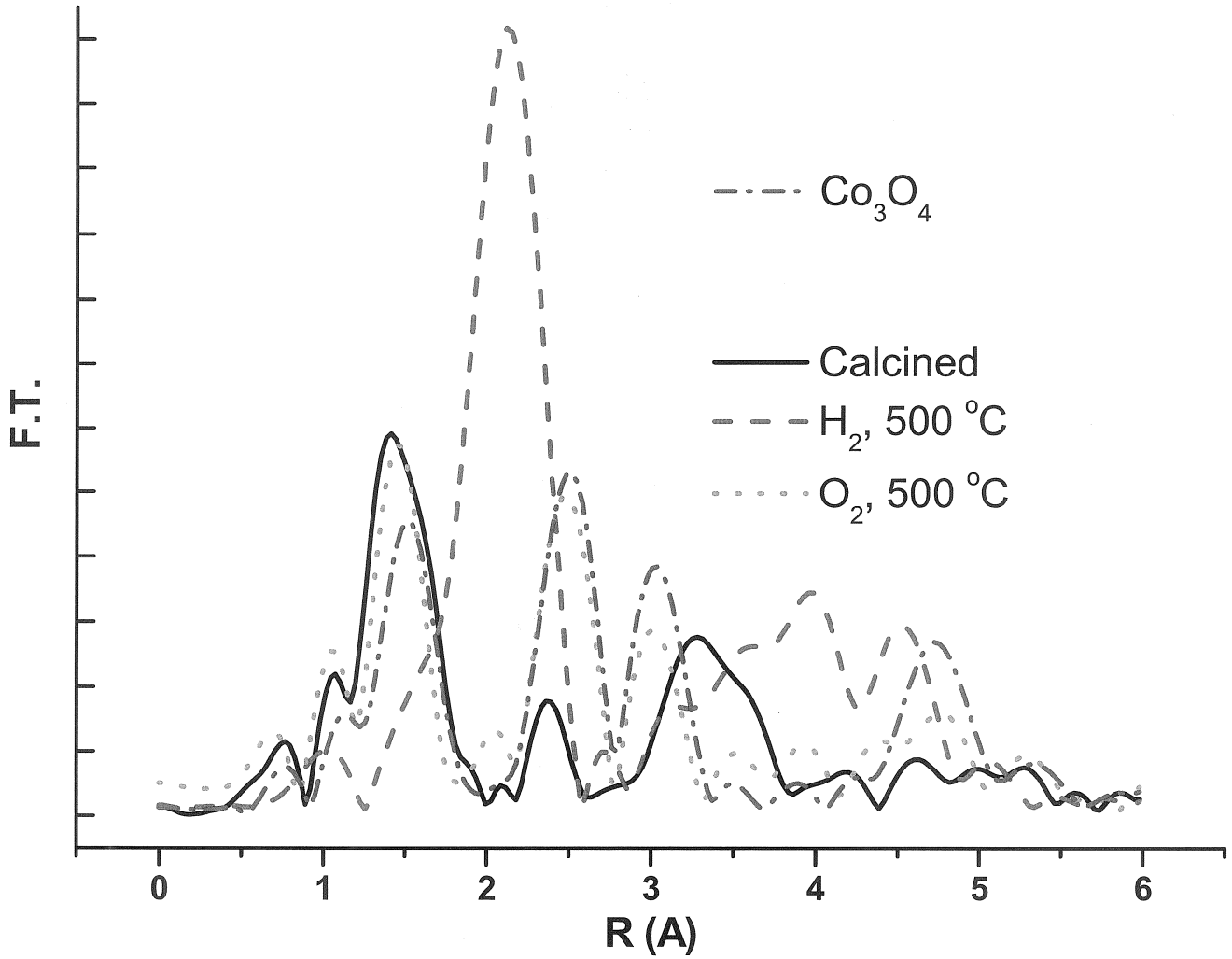

Figure 8

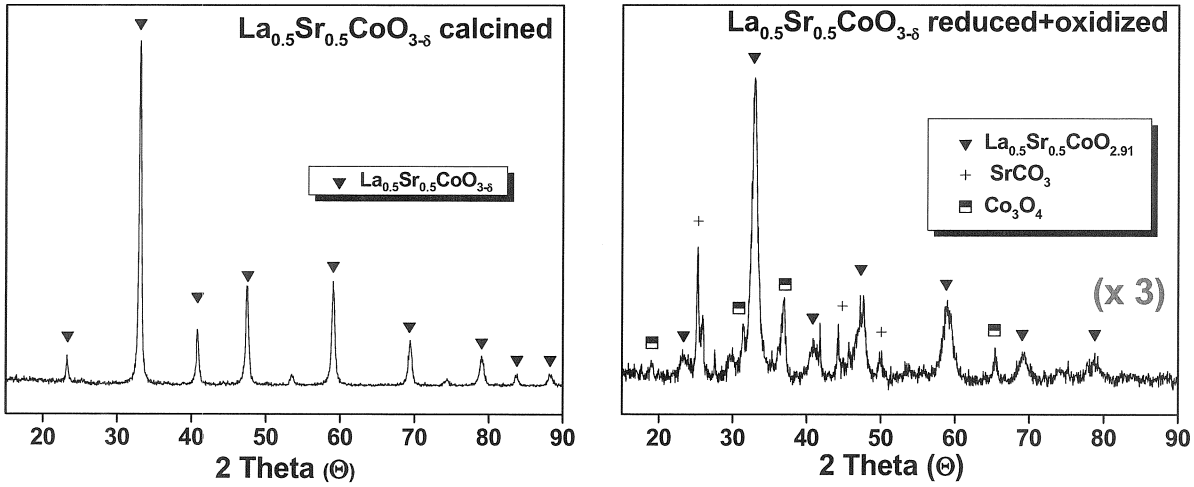
La0.5Sr0.5CoO3-δ calcined
La0.5Sr0.5CoO3-δ
20 30 40 50 60 70 80 90
2 Theta (Θ)
La0.5Sr0.5CoO3-δ reduced+oxidized
La0.5Sr0.5CoO2.91
SrCO3
Co3O4
(x 3)
20 30 40 50 60 70 80 90
2 Theta (Θ)

Figure 9

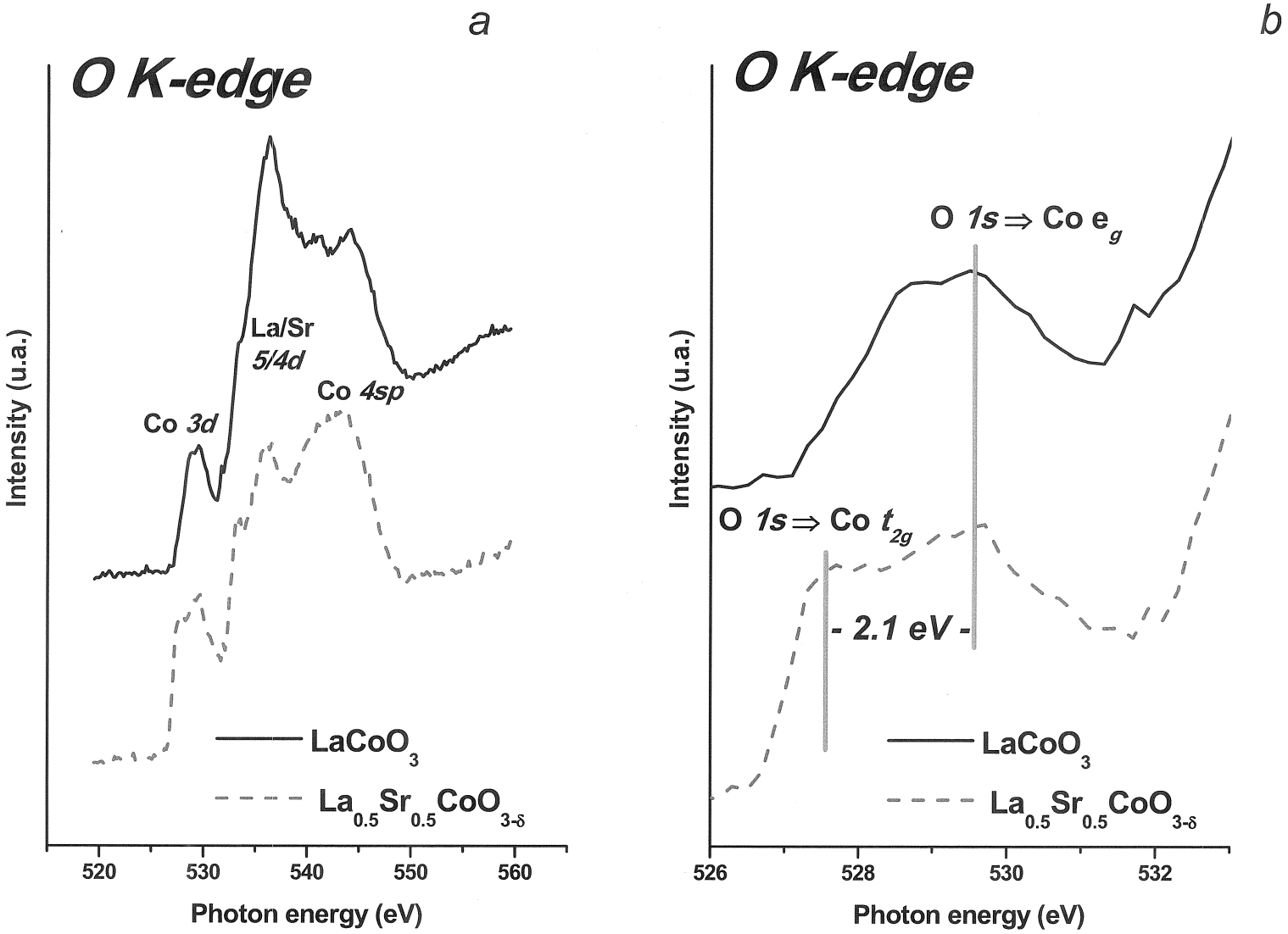
a
O K-edge
Intensity (u.a.)
La/Sr
5/4d
Co 4sp
Co 3d
LaCoO3
La0.5Sr0.5CoO3-δ
520
530
540
550
560
Photon energy (eV)
b
O K-edge
Intensity (u.a.)
O 1s ⇒ Co eg
O 1s ⇒ Co t2g
- 2.1 eV -
LaCoO3
La0.5Sr0.5CoO3-δ
526
528
530
532
Photon energy (eV)

Figure 10

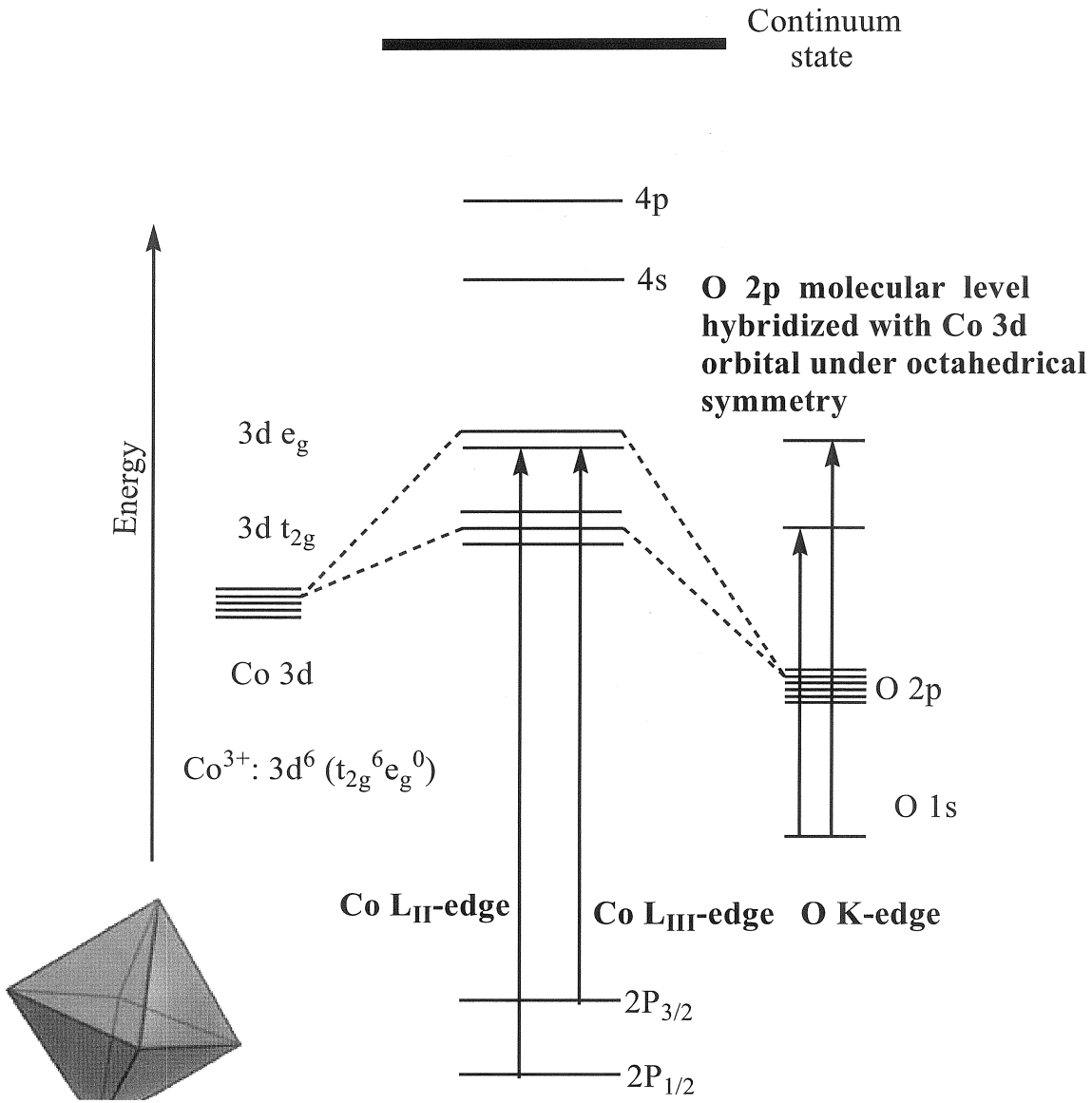
Continuum state
4p
4s
O 2p molecular level hybridized with Co 3d orbital under octahedrical symmetry
Energy
3d e_g
3d t_{2g}
Co 3d
Co^{3+}: $3d^6$ ($t_{2g}^6 e_g^0$)
O 2p
O 1s
Co L_{II}-edge
Co L_{III}-edge
O K-edge
$2P_{3/2}$
$2P_{1/2}$

Scheme 1